

**Raman mapping of atomic hydrogen and oxygen in the Orion Bar and Orion South**WILLIAM J. HENNEY<sup>1</sup><sup>1</sup>*Instituto de Radioastronomía y Astrofísica, Universidad Nacional Autónoma de México, Apartado Postal 3-72, 58090 Morelia, Michoacán, Mexico***Abstract**

I show that the broad Raman-scattered wings of H $\alpha$  can be used to map neutral gas illuminated by high-mass stars in star forming regions. The near wings ( $\Delta\lambda \approx \pm 10$  Å) trace neutral hydrogen columns of about  $5 \times 10^{20} \text{ cm}^{-2}$ , while the farther wings ( $|\Delta\lambda| > 30$  Å) trace columns of about  $5 \times 10^{21} \text{ cm}^{-2}$ . Absorption features in the pseudo-continuum at 6633 and 6664 Å correspond to neutral oxygen far-ultraviolet absorption lines at 1027.43 Å and 1028.16 Å.

**Keywords:** Atomic physics; Radiative transfer; Photodissociation regions

**1. INTRODUCTION**

Raman scattering is the inelastic analog of Rayleigh scattering by atoms or molecules. Both processes begin with a radiation-induced transition of an electron to a virtual bound state (non-eigenstate)

non-resonant scattering Recently, Dopita et al. (2016) identified Raman scattering wings to the H $\alpha$  line in the Orion Nebula and a number of H II regions in the Magellanic Clouds.

Dopita et al. (2016) propose that the Raman wings form at the transition zone near the ionization fronts in H II regions. However, the total neutral hydrogen column through the ionization front can be no more than about  $10/\sigma_0 \approx 2 \times 10^{18} \text{ cm}^{-2}$ , where  $\sigma_0 \approx 6.3 \times 10^{-18} \text{ cm}^2$  is the ground-state hydrogen photoionization cross section at threshold (Osterbrock & Ferland 2006). The Raman scattering cross section at wavelengths responsible for the observed wings is much lower than this:  $\sigma_{\text{Raman}} \sim 10^{-22} \text{ cm}^2$  (Chang et al. 2015), meaning that the Raman scattering optical depth through the ionization front is only of order 0.0001. A vastly larger column density of neutral hydrogen is available in the photodissociation region outside the ionization front, so it is more likely that Raman scattering will occur there instead, so long as there is sufficient far ultraviolet radiative flux in the vicinity of the Lyman  $\beta$  line (1025 Å).

**2. SPECTRAL MAPPING OF RAMAN WINGS**

MUSE (Bacon et al. 2010) observations of the Orion Nebula (Weilbacher et al. 2015; McLeod et al. 2015).

**3. RAMAN SCATTERING OF SPECTRAL LINES**

When a photon is Raman-scattered from the vicinity of Ly $\beta$  (UV domain) to the vicinity of H $\alpha$  (optical domain) its wavelength is transformed from  $\lambda_1$  to  $\lambda_2$ . Intervals in frequency ( $\nu = c/\lambda$ ) or wavenumber ( $\tilde{\nu} = 1/\lambda$ ) space are conserved between the two domains. For example the wavenumber displacement from the H I line center can be written in two ways:

$$\Delta\tilde{\nu} = \tilde{\nu}_1 - \tilde{\nu}(\text{Ly}\beta) = \tilde{\nu}_2 - \tilde{\nu}(\text{H}\alpha), \quad (1)$$

from which it follows that

$$\lambda_2 = \left( \frac{1}{\lambda(\text{H}\alpha)} + \frac{1}{\lambda_1} - \frac{1}{\lambda(\text{Ly}\beta)} \right)^{-1}. \quad (2)$$

All wavelengths are on the vacuum scale unless otherwise noted. An example is given in Table 3 for the rest wavelengths of transitions between the ground  $2s^22p^4 \ ^3P$  configuration of neutral  $^{16}\text{O}$  and the excited  $2s^22p^33d \ ^3D$  configuration. The O I data is obtained from highly accurate laser metrology (Ivanov et al. 2008; Marinov et al. 2017), with a precision of  $0.08 \text{ cm}^{-1}$  or better. The fine structure splitting of the excited state ( $\sim 0.1 \text{ cm}^{-1}$ ) is much smaller than of the ground state ( $\sim 100 \text{ cm}^{-1}$ ), so that the 6 transitions fall into 3 well-separated groups. The three transitions from the lowest energy  $J_i = 2$  level are very close to Ly $\beta$  ( $\Delta\tilde{\nu} \approx 4 \text{ cm}^{-1}$ ), whereas the two transitions from  $J_i = 1$  ( $\Delta\tilde{\nu} \approx 162 \text{ cm}^{-1}$ ) and the single transition from  $J_i = 0$  ( $\Delta\tilde{\nu} \approx 231 \text{ cm}^{-1}$ ) lie increasingly to the red. The corresponding wavelengths in the optical domain,  $\lambda_2$ , are therefore on the red side of H $\alpha$ . The final column of the table uses STP refractive indices (Greisen et al. 2006) to convert  $\lambda_2$  to air wavelengths,  $\lambda_{\text{air}}$ , for ease of comparison with ground-based optical spectroscopy. The resultant wavelength is 6663.747 Å for the  $J_i = 0$  line, with an uncertainty of about 0.004 Å, which is much smaller than typical observational precision (for instance, 0.07 Å for a very high resolution spectrograph with resolving power of  $R = 10^5$ ).

**Table 1.** Wavelength bands used for extracting Raman-scattered light

**Figure 1.** Spatial distribution of Raman-scattered wings in  $H\alpha$

The two  $J_i = 1$  lines, with a separation of  $0.028 \text{ \AA}$ , will always be blended in observations, giving a mean wavelength of  $6633.347 \text{ \AA}$  (assuming the upper levels are distributed according to statistical weight  $2J_k + 1$ ). Similarly, the three  $J_i = 2$  lines have a mean wavelength of  $6564.386 \text{ \AA}$ , but this is so close to  $H\alpha$  (corresponding to a Doppler shift of  $75 \text{ km s}^{-1}$ ) that it would be very difficult to observe.

The  $6633 \text{ \AA}$  and  $6664 \text{ \AA}$  lines are clearly detected in the MUSE spectra as absorption features against the pseudo-continuum of the broad  $H\alpha$  wings (see Fig XX), although the latter is blended with a  $\text{Ni II}$  emission line at  $6666.8 \text{ \AA}$ . This is further proof of the Raman scattering nature of the wings.

#### 4. HIGH-RESOLUTION SPECTROSCOPY OF RAMAN-SCATTERED $\text{O I } 1028 \text{ \AA}$

Keck HIRES spectra described in Henney & O'Dell (1999) and Bally et al. (2000). The spectrum I use is of HH 529 base region in Orion South. Published results from these data have concentrated on strong nebular lines, but here I use a small section of the spectrum in the range  $6660 \text{ \AA}$  to  $6670 \text{ \AA}$  for reasons which will become apparent.

#### 5. DISCUSSION

The effective resolving power of the optical spectrograph is multiplied by 6.4 for the FUV domain.

The  $\text{O I}$  lines should be in absorption in the spectrum seen by the Raman scatterers.

Salgado et al. (2016) had found low dust cross-section in Orion Bar PDR, but there are loopholes. First, they assume plane-parallel geometry with exactly edge-on viewing angle, while in reality it is a roughly cylindrical filament. Second, they ignore scattering, see Watson et al. (1998).

Geometry of bar: in Henney et al. (2005) I pointed out that a diverging cylindrical geometry is necessary to explain the sharp peak in the  $[\text{N II}]$  emissivity seen at the ionization front. It has been apparent since O'Dell & Yusef-Zadeh (2000) that the nebula contains many bar-like features.

Even for high PDR optical depth, no multiple Raman scattering will occur since the population of  $2s$  is very small and the post-scattered photons have insufficient energy to excite any transitions from  $1s$ .

#### REFERENCES

- Bacon, R., Accardo, M., Adjali, L., et al. 2010, in Society of Photo-Optical Instrumentation Engineers (SPIE) Conference Series, Vol. 7735, Proc. SPIE, 773508, doi: [10.1117/12.856027](https://doi.org/10.1117/12.856027)
- Bally, J., O'Dell, C. R., & McCaughrean, M. J. 2000, AJ, 119, 2919, doi: [10.1086/301385](https://doi.org/10.1086/301385)
- Chang, S.-J., Heo, J.-E., Di Mille, F., et al. 2015, ApJ, 814, 98, doi: [10.1088/0004-637X/814/2/98](https://doi.org/10.1088/0004-637X/814/2/98)
- Dopita, M. A., Nicholls, D. C., Sutherland, R. S., Kewley, L. J., & Groves, B. A. 2016, ApJL, 824, L13, doi: [10.3847/2041-8205/824/L13](https://doi.org/10.3847/2041-8205/824/L13)
- Greisen, E. W., Calabretta, M. R., Valdes, F. G., & Allen, S. L. 2006, A&A, 446, 747, doi: [10.1051/0004-6361:20053818](https://doi.org/10.1051/0004-6361:20053818)
- Henney, W. J., Arthur, S. J., Williams, R. J. R., & Ferland, G. J. 2005, ApJ, 621, 328, doi: [10.1086/427491](https://doi.org/10.1086/427491)
- Henney, W. J., & O'Dell, C. R. 1999, AJ, 118, 2350, doi: [10.1086/301087](https://doi.org/10.1086/301087)
- Ivanov, T. I., Salumbides, E. J., Vieitez, M. O., et al. 2008, MNRAS, 389, L4, doi: [10.1111/j.1745-3933.2008.00507.x](https://doi.org/10.1111/j.1745-3933.2008.00507.x)
- Marinov, D., Booth, J. P., Drag, C., & Blondel, C. 2017, Journal of Physics B Atomic Molecular Physics, 50, 065003, doi: [10.1088/1361-6455/aa5a88](https://doi.org/10.1088/1361-6455/aa5a88)
- McLeod, A. F., Weilbacher, P. M., Ginsburg, A., et al. 2015, ArXiv e-prints. <https://arxiv.org/abs/1511.01914>
- O'Dell, C. R., & Yusef-Zadeh, F. 2000, AJ, 120, 382, doi: [10.1086/301429](https://doi.org/10.1086/301429)
- Osterbrock, D. E., & Ferland, G. J. 2006, Astrophysics of gaseous nebulae and active galactic nuclei, 2nd edn. (Sausalito, CA: University Science Books)
- Salgado, F., Berné, O., Adams, J. D., et al. 2016, ApJ, 830, 118, doi: [10.3847/0004-637X/830/2/118](https://doi.org/10.3847/0004-637X/830/2/118)
- Watson, A. M., Henney, W. J., & Escalante, V. 1998, in American Astronomical Society Meeting Abstracts, Vol. 193, 16.03
- Weilbacher, P. M., Monreal-Ibero, A., Kollatschny, W., et al. 2015, A&A, 582, A114, doi: [10.1051/0004-6361/201526529](https://doi.org/10.1051/0004-6361/201526529)

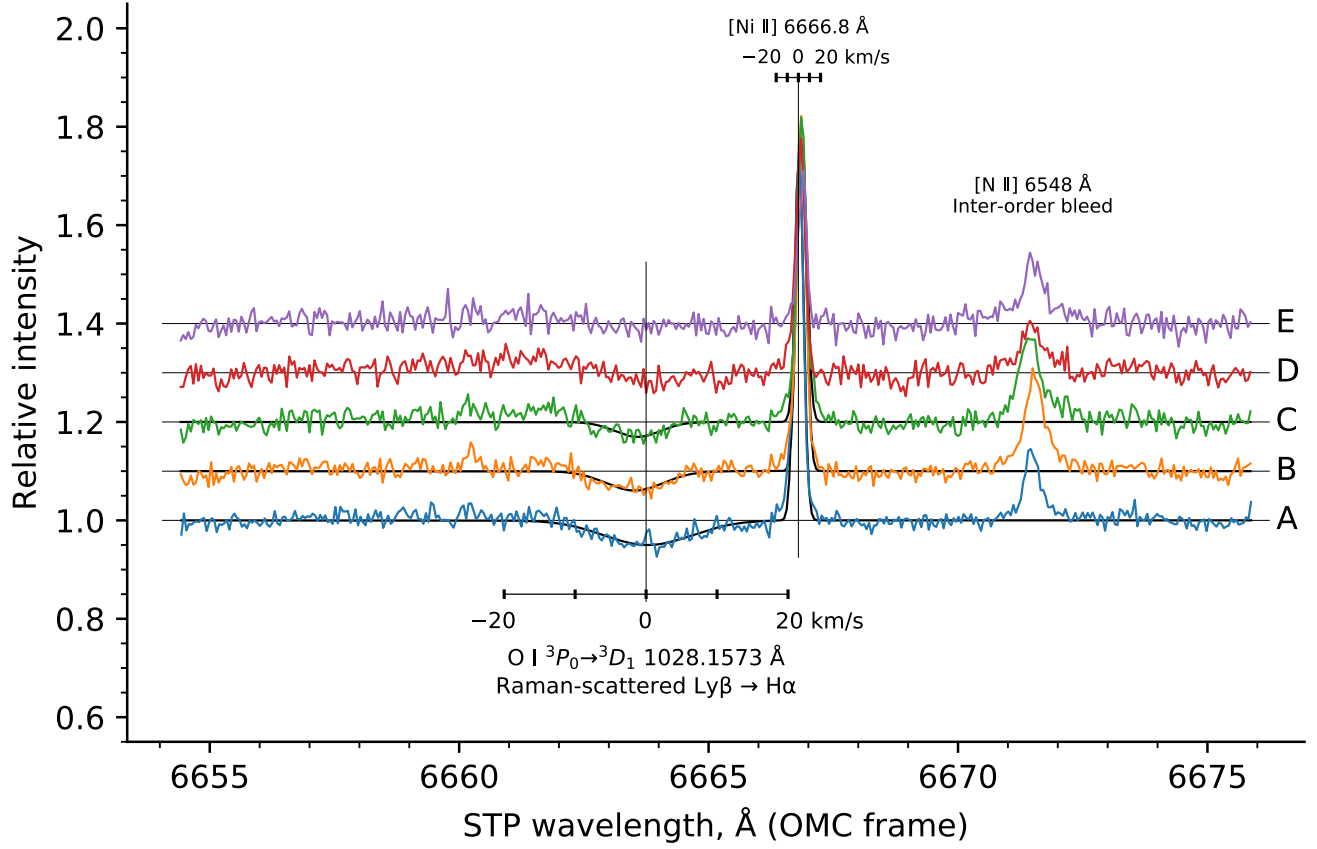


**Figure 2.** Keck HIRES spectra of Raman-scattered O I absorption line for five regions in Orion South. Wavelengths are given on an air scale and in the rest-frame of the Orion Molecular Cloud, as defined by the peak velocity of  $^{13}\text{CO}$ .

**Table 2.** FUV/optical wavelength equivalencies for Raman scattering

| Ion | Transition   | $J_i \rightarrow J_k$                              | $\lambda_1, \text{\AA}$        | $\tilde{\nu}_1, \text{cm}^{-1}$ | $\Delta\tilde{\nu}, \text{cm}^{-1}$ | $\tilde{\nu}_2, \text{cm}^{-1}$  | $\lambda_2, \text{\AA}$ | $\lambda_{\text{air}}, \text{\AA}$ |
|-----|--|--|--------------------------------|---------------------------------|-------------------------------------|----------------------------------|-------------------------|------------------------------------|
|     |  |  | .... Ly $\beta$ , $n = 1$ .... |                                 |                                     | ..... H $\alpha$ , $n = 2$ ..... |                         |                                    |
| H I | $ns\ ^2S \rightarrow 3p\ ^2P$                      | $\frac{1}{2} \rightarrow \frac{1}{2}, \frac{3}{2}$ | 1025.72220                     | 97492.283                       | 0.000                               | 15233.329                        | 6564.553                | 6562.740                           |
| O I | $2s^2 2p^4\ ^3P \rightarrow 2s^2 2p^3(^4S)3d\ ^3D$ | $0 \rightarrow 1$                                  | 1028.15729                     | 97261.383                       | -230.900                            | 15002.429                        | 6665.587                | 6663.747                           |
|     |  | $1 \rightarrow 1$                                  | 1027.43139                     | 97330.100                       | -162.183                            | 15071.146                        | 6635.196                | 6633.364                           |
|     |  | $1 \rightarrow 2$                                  | 1027.43077                     | 97330.159                       | -162.124                            | 15071.205                        | 6635.170                | 6633.338                           |
|     |  | $2 \rightarrow 1$                                  | 1025.76339                     | 97488.369                       | -3.914                              | 15229.415                        | 6566.240                | 6564.427                           |
|     |  | $2 \rightarrow 2$                                  | 1025.76276                     | 97488.429                       | -3.854                              | 15229.475                        | 6566.215                | 6564.401                           |
|     |  | $2 \rightarrow 3$                                  | 1025.76170                     | 97488.530                       | -3.753                              | 15229.576                        | 6566.171                | 6564.358                           |

**Table 3.** Fit parameters from Gaussian line fits

| Region | O I      |          |          | Ni II    |          |          |
|--------|----------|----------|----------|----------|----------|----------|
|        | <i>A</i> | <i>V</i> | $\sigma$ | <i>A</i> | <i>V</i> | $\sigma$ |
| A      |          |          |          |          |          |          |
| B      |          |          |          |          |          |          |
| C      |          |          |          |          |          |          |
| D      |          |          |          |          |          |          |
| E      |          |          |          |          |          |          |